• Data Description Article •

High-resolution Projection Dataset of Agroclimatic Indicators over Central Asia

Yuan QIU, Jinming FENG*, Zhongwei YAN, and Jun WANG

Key Laboratory of Regional Climate-Environment for Temperate East Asia (RCE-TEA),

Institute of Atmospheric Physics, *Chinese Academy of Sciences*, *Beijing* 100029, *China*

ABSTRACT

To understand the potential impacts of projected climate change on the vulnerable agriculture in Central Asia (CA), six agroclimatic indicators are calculated based on the 9-km-resolution dynamical downscaled results of three different global climate models from Phase 5 of the Coupled Model Intercomparison Project (CMIP5), and their changes in the near-term future (2031–50) are assessed relative to the reference period (1986–2005). The quantile mapping (QM) method is applied to correct the model data before calculating the indicators. Results show the QM method largely reduces the biases in all the indicators. Growing season length (GSL, day), summer days (SU, day), warm spell duration index (WSDI, day), and tropical nights (TR, day) are projected to significantly increase over CA, and frost days (FD, day) are projected to decrease. However, changes in biologically effective degree days (BEDD, °C) are spatially heterogeneous. The high-resolution projection dataset of agroclimatic indicators over CA can serve as a scientific basis for assessing the future risks to local agriculture from climate change and will be beneficial in planning adaption and mitigation actions for food security in this region.

Key words: agroclimatic indicators, Central Asia, near-term future, agriculture, quantile mapping

---

	Database profile
Database title	High-resolution projection dataset of agroclimatic indicators over Central Asia (1986–2005 and 2031–50)
Time range	Reference (historical) period: 1986–2005; Future period: 2031–50.
Geographical scope	Central Asia (36°–94°E, 30°–58°N)
Data format	netCDF4
Data volume	132 MB
Data service system	National Tibetan Plateau Data Center (https://doi.org/10.11888/Atmos.tpdc.271934)
Sources of funding	The Strategic Priority Research Program of Chinese Academy of Sciences (Grand No. XDA20020201); The General Project of the National Natural Science Foundation of China (Grand No. 41875134); The TianHe Qingsuo Project – special fund project in the field of climate, meteorology and ocean.
Database composition	1. The dataset contains six agroclimatic indicators (GSL, BEDD, FD, SU, WSDI, and TR); 2. Files for each indicator are grouped in a directory; 3. The values for each simulation period (1986–2005 and 2031–50) and each experiment (WRF_MPI_COR, WRF_CCSM_COR, and WRF_Had_COR) are stored in a file. 4. The names of the files follow the order: [experiment_name].[indicator_name].[period].nc

1. Introduction

Central Asia (referred to as CA, Fig. 1), which consists of five countries (Kazakhstan, Kyrgyzstan, Tajikistan, Turkmenistan, and Uzbekistan), is highly agrarian, with 60% of its population living in rural areas and agriculture accounting for over 45% of total employment and nearly 25% of the Gross Domestic Production (Babu and Djalalov, 2006). Agricultural land in this region is mostly desert and mountainous pastures. Arable land suitable for crop production is about 20% of the agricultural land (and as low as 4% in Turkmenistan). The main crops produced in CA are cotton and wheat. Kazakhstan is one of the world's major wheat and

---

* Corresponding author: Jinming FENG
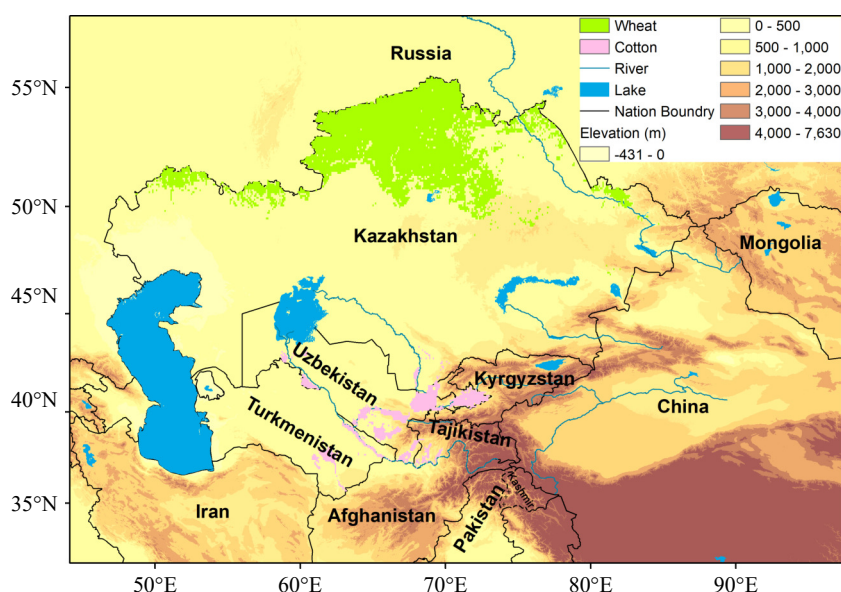 Email: fengjm@tea.ac.cn

Fig. 1. Study area and its surroundings. The main producing area of wheat (cotton) in Central Asia is colored by green (pink).

flour exporters. Uzbekistan is the sixth largest producer and the second largest exporter of cotton in the world. Semi-arid to arid climates prevail in the lowland areas of CA. Thus, in the central and western parts of CA, agriculture is only possible with irrigation. Major areas under rainfed agriculture are only found in the very north of Kazakhstan (Sommer et al., 2013). Every year, natural disasters such as droughts and extreme temperatures (cold and heat waves) bring risks to agricultural production in this region (Thurman, 2011).

As one of the hot spots of climate change (Giorgi, 2006), CA has experienced a significant warming (0.16°C (10 yr)⁻¹) during the past century (1901–2003, Chen et al., 2009), with an accelerating warming rate (0.36°C–0.42°C per decade) in the past ~30 years (1979–2011, Hu et al., 2014). Meanwhile, its annual precipitation has increased (Chen et al., 2011; Hu et al., 2017). The warming and wetting trend is very likely to be ongoing in the future with the increase of heatwave and drought events (Mannig et al., 2013; Huang et al., 2014; Ozturk et al., 2017; Peng et al., 2019; Jiang et al., 2020b; Zhu et al., 2020; Qiu et al., 2022).

Climate change may pose challenges to the vulnerable agriculture in CA. Sommer et al. (2013) assessed the impacts of projected climate change on wheat in this region and found that the projected increase in temperature is the most important factor leading to earlier and faster crop growth and higher biomass accumulation and yield. Conversely, the projected increase in precipitation is expected to be insignificant because of the increasing evaporative demand of the crops. In addition, higher temperatures were found to bring an increased risk of flower sterility and thus lead to less yields. Mirzabaev (2018) suggested adaptive actions should be taken to strengthen the resilience of agriculture producers in CA to increased weather variability.

Due to the lack of high-resolution climate data and less

attention from the community relative to its surrounding areas, like East Asia, South Asia, and the Mediterranean (Wang et al., 2009; Piao et al., 2010; Iglesias et al., 2011; Bandara and Cai, 2014; Cramer et al., 2018; Aryal et al., 2020; Huang et al., 2020), studies on the impacts of climate change on agriculture in CA are lacking, especially on the potential impacts of projected climate change under warming scenarios in the near-term future.

Recently, we carried out a study that involves the dynamical downscaling of multiple global climate models (GCMs) for the CA region with an unprecedented horizontal resolution of 9 km (Qiu et al., 2022). The reference and future periods of the simulations are 1986–2005 and 2031–50, respectively. In this study, the model data from the downscaled results is applied to calculate some key agroclimatic indicators (referred to as AIs), which are proxies for the effect of weather and climate on specific agricultural activities (Arnell and Freeman, 2021) and both practical and understandable to farmers and policy makers (Trnka et al., 2011). As absolute threshold-based temperature indices are largely sensitive to systematic model biases, statistical bias correction (adjustment) methods are suggested to be used to correct the raw model outputs (Dosio, 2016: Iturbide et al., 2022). Here, the quantile mapping method (Themeßl et al., 2011) is applied to correct the simulated temperature before calculating the AIs relating to absolute temperature thresholds.

The aim of this paper is to describe the high-resolution projection dataset of AIs over CA and investigate projected changes in these indicators in the near-term future. This study can serve as a scientific basis for assessing the future risks to the local agriculture from climate change and will be beneficial in planning adaption and mitigation actions for food security in this region. The remainder of this paper is organized as follows: section 2 describes the data and meth-

ods. Projected changes in the indicators are presented in section 3, as well as the evaluation of the QM method. Section 4 provides usage notes. Discussion and conclusion are in section 5.

2. Data and method

2.1. *The model data*

The AIs assessed in this study are calculated based on daily mean/maximum/minimum temperature (TG/TX/TN) from the 9-km-resolution dynamical downscaling of three different GCMs in CA with a regional climate model (RCM), the Weather Research and Forecasting (WRF) model (Skamarock et al., 2008). The three GCMs are MPI-ESM-MR (referred to as MPI), CCSM4 (CCSM), and HadGEM2-ES (Had) from Phase 5 of the Coupled Model Intercomparison Project (CMIP5). Before the downscaling, the bias-correction technique developed by Bruyère et al. (2014) is utilized to correct the climatology of the GCMs and meanwhile allow synoptic and climate variability to change. The WRF simulations are labeled as MPI_WRF_COR, CCSM_WRF_COR, and Had_WRF_COR ("COR" means using the bias-correction technique), respectively. The reference-period simulations are from 1986 to 2005, and the future runs are between 2031 and 2050 under the moderate emission scenario RCP 4.5.

The simulated TG/TX/TN over CA has been extensively evaluated, and basic features of the projected temperature changes have been investigated (Qiu et al., 2022a, 2022b). Results show that the RCM simulations driven by three different GCMs can well capture the local temperature on time scales from daily to annual in CA during the reference period. For instance, the spatial correlation coefficients (SCCs) of the simulated seasonal and annual mean TG/TX/TN over CA are all above 0.95 against the observations, and their root mean square errors (RMSEs) are all below 2.50°C. The three WRF simulations indicate that annual mean TG averaged over CA will increase by 1.6°C–2.0°C in the near-term future (2031–50) relative to the reference period (1986–2005). Stronger warming is detected north of ~45°N

in CA from autumn to spring. Enhanced warming is projected in many mountainous regions (like the Tibetan Plateau/ Himalayas and Alps) around the world (Rangwala et al., 2013; Mountain Research Initiative EDW Working Group, 2015; Palazzi et al., 2019). However, the projected warming in the high-elevation areas of CA is not stronger than that in the plain areas.

2.2. *Agroclimatic indicators*

Specific crops grow well in specific climate regions, and the success of a crop can be related to climate factors (e. g., frequency of frost damage, length of growing season, heat stress) as well as physical factors (e.g., soil, slope, aspect) and farm management (e.g., irrigation, fertilization) (Petr, 1991; Rijks, 1994; Holden and Brereton, 2004). Understanding the complex interactions between crops and regional climate allows for better management decisions (Trnka et al., 2011). AIs are widely used to convey climate variability and change, which are meaningful to the agricultural sector. For instance, the Global Agriculture Sectoral Information System project developed by the European Centre for Medium-Range Weather Forecasts (ECMWF) has produced contemporary and future AIs for climate change impact studies for global agriculture (SIS, 2019).

Here, we chose six of the ECMWF indicators that are most meaningful to assessing the potential impact of projected climate change on the agriculture in CA. Among them, growing season length (GSL, day) refers to the number of days when plant growth takes place, biologically effective degree days (BEDD, °C) provides valuable information on the local heat summation, frost days (FD, day) indicates frost damage, summer days (SU, day) and warm spell duration index (WSDI, day) indicate heat stress and heatwaves, and tropical nights (TR, day) gives information about the occurrence of various pests. Table 1 shows the detailed definitions of these AIs, which are calculated using TG/TX/TN from the WRF simulations (MPI_WRF_COR, CCSM_WRF_COR, and Had_WRF_COR). Note that GSL is calculated with the model data throughout the year, and the other indicators are calculated for the growing season (April to October, Gessner et al., 2013).

Table 1. Information about the agroclimatic indicators used in the study.

Name	Unit	Definition
Growing season length (GSL)	d	Number of days between the first occurrence after 1 January of at least six consecutive days with TG >5°C and the first occurrence after 1 July of at least six consecutive days with TG < 5°C. This indicator refers to the number of days when plant growth takes place.
Biologically effective degree days (BEDD)	°C	Sum of TG above 10 °C and less than 30 °C. This indicator provides valuable information on the local heat summation.
Frost days (FD)	d	Number of days when TN < 0°C. This indicator provides information on frost damage.
Summer days (SU)	d	Number of days when TX > 25°C. This indicator provides an indication of the occurrence of heat stress.
Warm spell duration index (WSDI)	d	Number of days with at least six consecutive days when TX > TX90th, where TX90th is the calendar day 90th percentile centered on a five-day window for the base period 1986–2005. This indicator provides an indication of the occurrence of heat stress.
Tropical nights (TR)	d	Number of days when TN > 20°C. This indicator provides an indication of occurrence of various pests.

The WRF simulations show that projected changes in precipitation over few areas are significant in CA in the near-term future (Qiu et al., 2022a, 2022b). We found that projected changes in AIs calculated based on precipitation (e.g., wet days, heavy precipitation days, and maximum number of consecutive wet/dry days) are also insignificant over most of CA. Therefore, only the results of the AIs which relate to temperature are presented in this paper.

2.3. *Quantile mapping for postprocessing the model data*

Our recent study (Qiu et al., 2022b) found that the WRF simulations have systematic biases in simulating the surface air temperature. For instance, the annual mean TG over the very northern part of Kazakhstan and the Pamirs exhibits a cold bias, and that over other areas generally exhibits a warm bias. All the chosen AIs except WSDI relate to absolute temperature thresholds (see their definitions in Table 1) and are particularly sensitive to the systematic biases in the model data. The biases in the raw model outputs can propagate down to the AIs, which may add uncertainties in the projected changes in them. Thus, the QM method is separately used to postprocess the simulated TG, TX, and TN. First, a transfer function depending on the quantile distribution is established by matching the model data with observations during the reference period (1986–2005). Then, the transfer function is applied to correct the model data in the future period (2031–50). The equations are as below:

$$F_{m,c}(x_{m,c}) = F_{o,c}(x_{o,c}) , \qquad (1)$$

$$x_{bc} = F_{o,c}^{-1}\left[F_{m,p}\left(x_{m,p}\right)\right] , \qquad (2)$$

where the model data and observations are denoted by m and o, respectively, calibration period and projection (future) period are denoted by c and p, respectively, x is the variable, F and F^{-1} are the empirical cumulative distribution function (ecdf) and its inverse, respectively, and x_{bc} is the bias-corrected model data. Numerous studies have found that the QM method can effectively remove model biases, not only for the mean and interannual variability, but also for extreme events (Ashfaq et al., 2010; Piani et al., 2010; Gudmundsson et al., 2012; Teutschbein and Seibert, 2012; Tong et al., 2021).

The land component of the fifth generation of European reanalysis (referred to as ERA5-Land, Hersbach et al., 2020) with ~9-km grid spacing is used as "observations" during the postprocessing. Prior to the bias correction, the model data is interpolated to the grid of the observations with the nearest neighbor method. There are two reasons why we chose ERA5-Land as observations. First, the traditional observations that are available for the CA region, like CRU TS v4 (version 4 of the Climatic Research Unit gridded Time Series) and CPC (Climate Prediction Center) Global daily temperature, have coarser resolution (0.5° × 0.5°) relative to the 9-km-resolution downscaled results. If we use these coarse-resolution gridded observations, the model data will be interpolated to their grids and the small-scale climate characteristics brought by the dynamical downscaling will be largely erased. Second, ERA5-Land is found to have good performance in describing the global land surface temperature with respect to the MODIS (Moderate Resolution Imaging Spectroradiometer) data (Hersbach et al., 2020) and has been applied for studies on many sectors in CA (Xue et al., 2019; Wang et al., 2020; Jiang et al., 2021; Lu et al., 2021).

2.4. *Main producing areas of wheat and cotton*

As introduced above, wheat and cotton are the main crops in CA. Hence, projected changes in the AIs over the main producing areas of these two crops are particularly assessed. Main producing areas of wheat and cotton are detected based on the Spatial Production Allocation Model (SPAM) 2010 v2.0 Global data (International Food Policy Research Institute, 2019), which contains the physical area, harvest area, production, and yield of 42 crops (including wheat and cotton) with 10 × 10-km grid-cell resolution. According to the condition that the main crop of a grid cell is defined as the crop whose harvest area is the largest and accounts for at least 5% of the grid cell area, the main producing area of wheat is detected to be located in northern Kazakhstan, with an area of ~3.8 × 10⁵ km², and that of cotton is detected to be along the Amu Darya and Syr Darya rivers and in Uzbekistan and Turkmenistan, with an area of ~9.4 × 10⁴ km² (Fig. 1). Other thresholds (3% and 7%) are also tested, and the results are similar to those with a threshold of 5%.

3. Results

3.1. *Evaluation of the quantile mapping method*

To evaluate the QM method, the reference period (1986–2005) of the model data is divided into two parts. The first half (1986–95) is set as the calibration period, during which the transfer function is established. The transfer function is then applied to correct the model data in 1996–2005. The AIs calculated based on the raw and bias-corrected model data (Raw-AIs and Cor-AIs) during 1996–2005 are compared with those calculated based on the observations (Obs-AIs) to show the performance of the QM method.

Figure 2 presents the time-averaged Obs-AIs (the left column) over CA during 1996–2005 and the biases of the time-averaged Raw-AIs (the middle column) and Cor-AIs (the right column). Because the spatial patterns of the biases are very consistent between the three WRF simulations (MPI_WRF_COR, CCSM_WRF_COR, and Had_WRF_COR), only the results of WRF_CCSM_COR are shown. It is seen that the application of the QM method caused drastic reductions in bias for all the indicators over CA, especially for BEDD and SU (Fig. 2e vs Fig. 2f, Fig. 2k vs Fig. 2l). The RMSEs of all the indicators are generally reduced by more than half. For instance, the ensemble mean of RMSEs of BEDD decreases from 289.86 °C per year to 96.08 °C per year (Fig. 3d), and that of SU decreases from 21.01 days

per year to 4.67 days per year (Fig. 3h). The Raw-AIs are close to the Obs-AIs in the spatial distribution, with the mean values of SCCs generally above 0.90 (e.g., Figs. 3a, c, and e). After using the bias correction, all the SCCs increase to near 1.00 (e.g., Fig. 3i), which suggests that the QM method not only reduces the biases of the AIs but also

brings improvements in describing their spatial patterns.

We also evaluated WSDI, which relates to relative (not absolute) temperature threshold (see its definition in Table 1) and is calculated based on the raw model data. We found that it is difficult for the regional model to accurately simulate the spatial distribution of WSDI in CA, with the
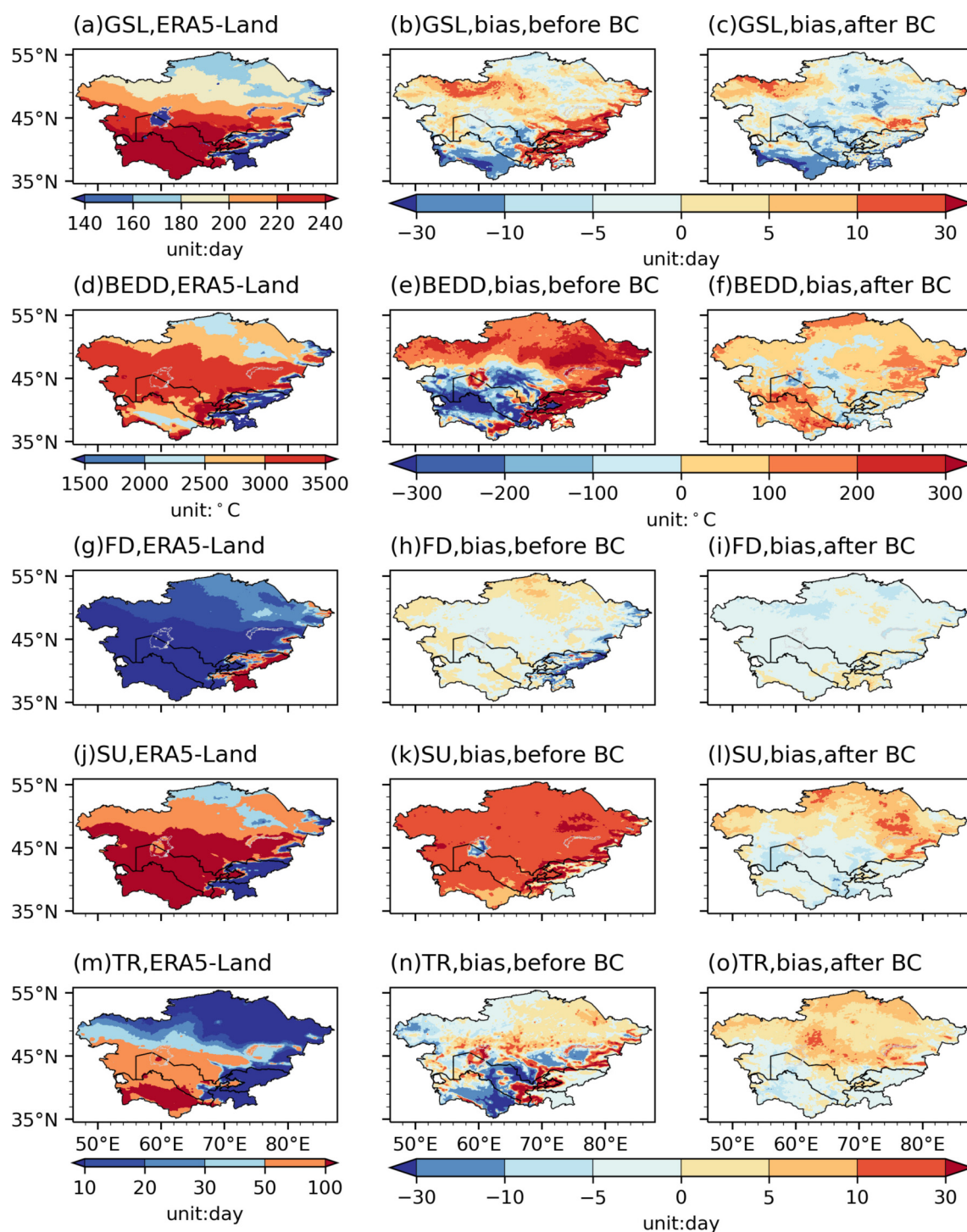

Fig. 2. The mean agroclimatic indicators (except WSDI) calculated based on ERA5-Land (the left column) during 1996–2005, the bias of the mean agroclimatic indicators calculated based on the model data before (the middle column) and after (the right column) bias correction (BC). The model data is from the simulation WRF_CCSM_COR.
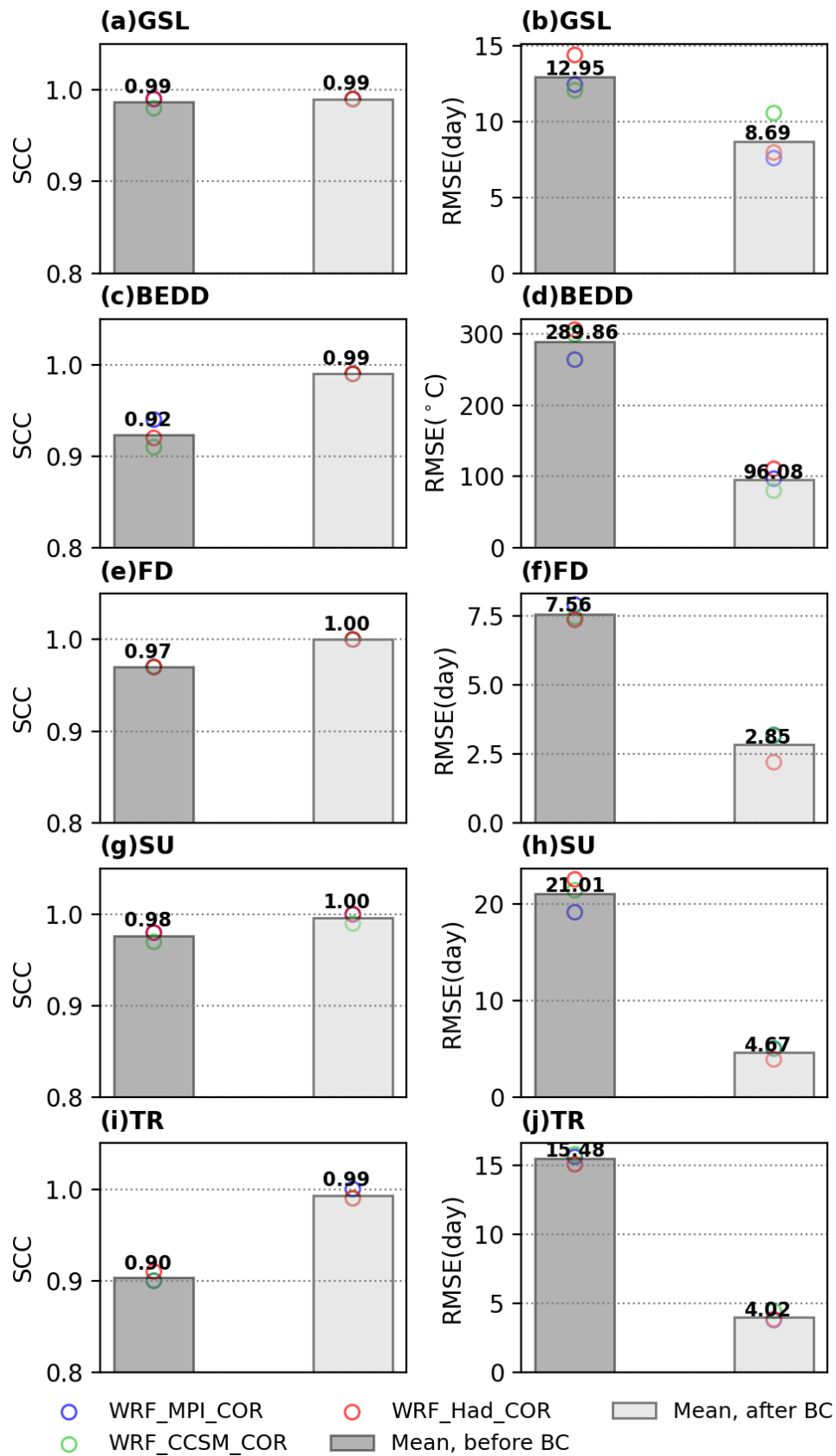
Fig. 3. Spatial correlation coefficients (SCCs) and root-mean-square errors (RMSEs) of the mean agroclimatic indicators (except WSDI) calculated based on the model data before and after bias correction (BC) in Central Asia during 1996–2005. The circles are the results of each simulation (WRF_MPI_COR, WRF_CCSM_COR, and WRF_Had_COR), and the bars are the mean values.

SCCs in the range of 0.3–0.4. However, the biases of WSDI are minor, with the RMSEs as low as about five days per year. To sum up, the QM method is excellent in improving the accuracy of the simulated AIs, which provides a good base for assessing the projected changes in the agroclimatic indicators in CA.

3.2. *Projected changes in the agroclimatic indicators*

Projected changes in the Cor-AIs during the future period (2031–50) relative to the reference period (1986–2005) are demonstrated in this section. Besides the results of each WRF simulation, the ensemble mean is also illustrated. Figures 4 and 5 show that GSL, SU, WSDI, and TR are projected to significantly increase over CA in the near-term future, while FD is very likely to decrease over the entire region, especially in the high-elevation areas (e.g., the Tien Shan and Pamirs). Averaged over CA, GSL changes from about 201–202 days per year (1986–2005) to around 213–217 days per year (2031–50, Table 2). The aver-

age number of SU (TR) increases from about 88 (35) days per year to around 101–108 (48–54) days per year. Moreover, the simulated WSDIs are 1.8–2.4 times longer in the coming decades. Regional averages of the Cor-AIs over the climate subregions [northern CA (NCA), middle CA (MCA), southern CA (SCA), and the mountainous areas (MT)] are also summarized in Table 2. See the scopes of these subregions in Fig. 1c of Qiu et al. (2022).

Figure 4 shows that BEDD increases (>100°C yr⁻¹) in northern CA and the mountainous areas and decreases (>300°C yr⁻¹) in the southern and middle parts of the plain areas. The reason why projected changes in BEDD are spatially heterogeneous is as follows: the northern part and mountain ranges of CA have relatively cold climates, and higher temperature in the future will lead to more days whose TG exceeds the lower limit (10°C) of BEDD and thus increases BEDD in these areas; in contrast, the southern and middle parts of the plain areas have relatively hot climates, and the local warming will cause more days whose TG goes over
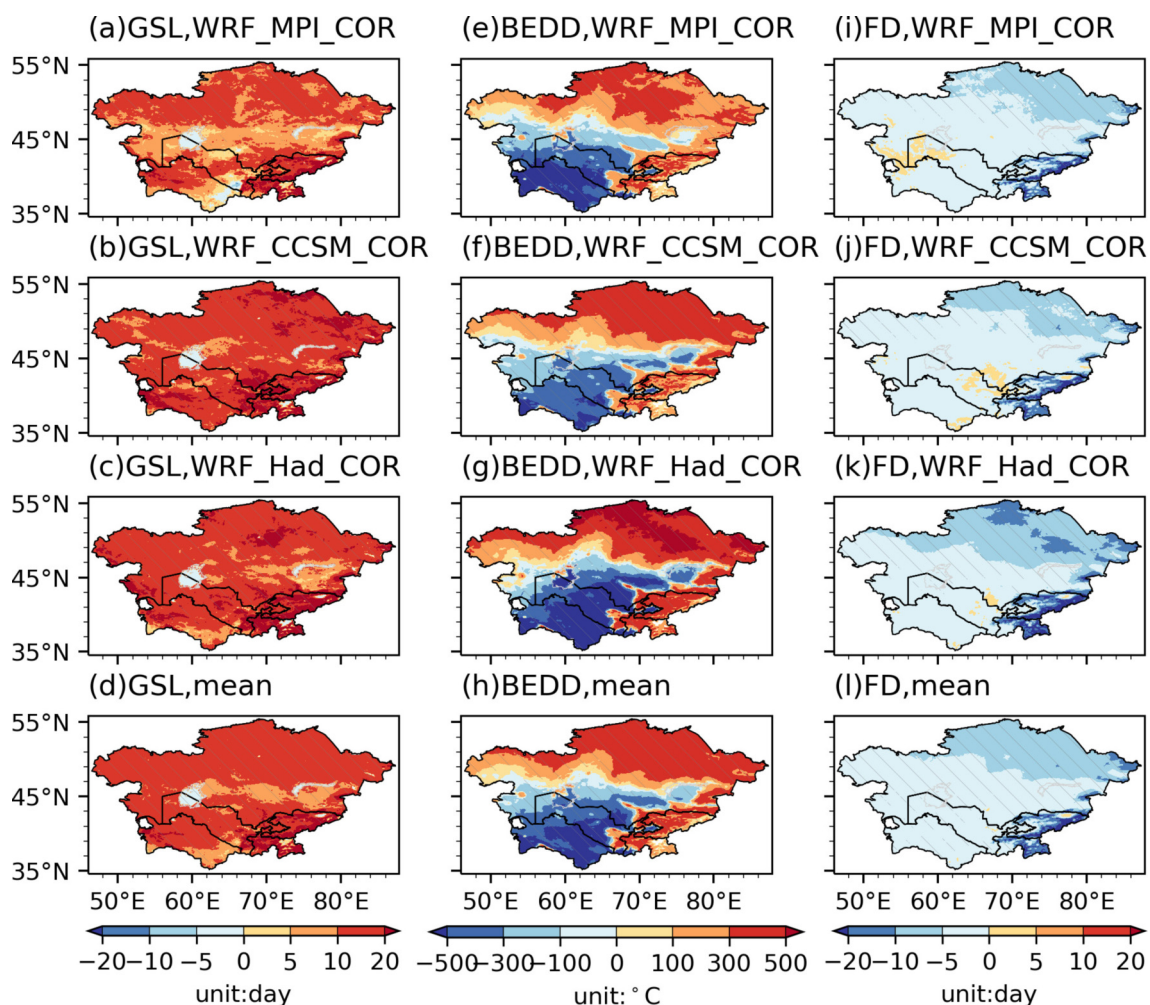

Fig. 4. Projected changes (2031–50 vs. 1986–2005) in GSL, BEDD, and FD calculated based on the bias-corrected model data from three WRF simulations (WRF_MPI_COR, WRF_CCSM_COR, and WRF_Had_COR). The ensemble means of the changes are also shown. The slashed areas in subplots a–c, e–g, and i–k indicate where the changes passed the significance test at the 95% confidence level using the two-tailed Student's *t*-test. The slashed areas in subplots d, h, and l indicate where the signals (+/−) of the changes in the WRF simulations are consistent.
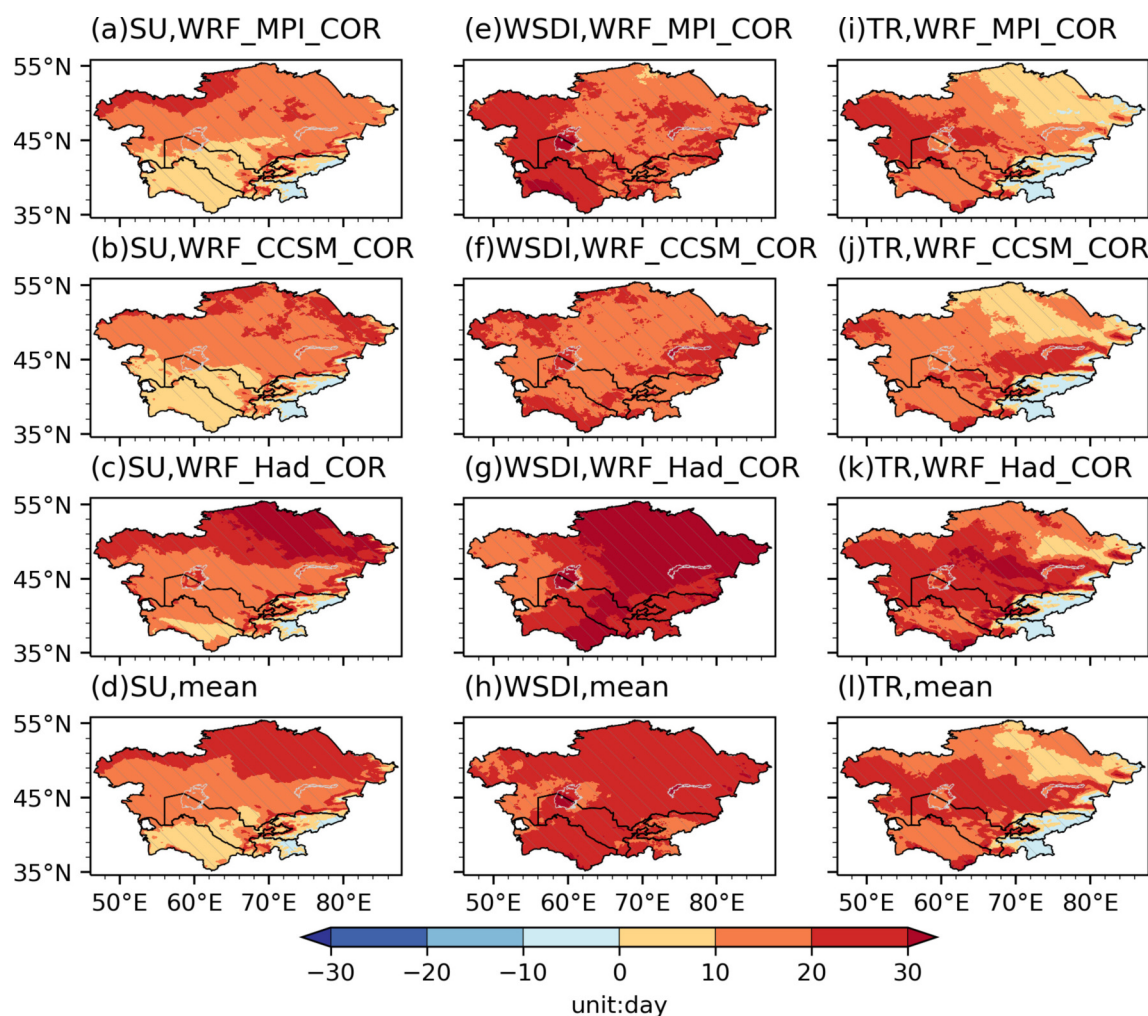
Fig. 5. Same as Fig.4, but for SU, WSDI, and TR.

the upper limit (30°C) of BEDD and thus reduces BEDD in these areas.

In particular, projected changes in the Cor-AIs over main producing areas of wheat and cotton are assessed. The ensemble mean of the results of the simulations shows that GSL, BEDD, SU, WSDI, and TR over the main producing area of wheat will increase by 8.7%, 15.6%, 49.8%, 112.1%, and 219.6%, respectively, and FD over this area will decrease by 40.7% (Fig. 6). Over the main producing area of cotton, GSL, SU, WSDI, and TR will increase by 3.9%, 6.5%, 91.0%, and 32.0%, respectively, and BEDD will decrease by 10.4%. There are few frost days in this area during the growing season both in the reference and future period. Prolonged growing seasons, more local heat summation, and less frost damage over the main producing area of wheat may increase crop yields. However, more summer days, warm spells, and tropical nights over the main producing areas of both wheat and cotton will increase the risk of heat stress and the occurrence of pests, which may cause less crop yields.

4. Usage notes

This dataset is hosted at the National Tibetan Plateau Data Center (tpdc.ac.cn/en/) (Qiu et al., 2022). The files are stored in netCDF4 format and compiled using the Climate and Forecast (CF) conventions. It contains six agroclimatic indicators calculated based on the TG/TX/TN from three WRF simulations (MPI_WRF_COR, CCSM_WRF_COR, and Had_WRF_COR) for a spatial domain covering the CA region and its surrounding areas. The spatial resolution is 0.1° × 0.1°. The dataset covers two continuous 20-year periods, 1986–2005 and 2031–50. The names of the files follow the order: [experiment_name].[variable_name].[period]. nc. For example, the file name, WRF_CCSM_COR.WSDI. 2031-2050.nc, represents the WSDI of the future period calculated based on the model data from the experiment WRF_CCSM_COR.

The original simulated TG/TX/TN is available at https://doi.org/10.11888/Meteoro.tpdc.271759 (Qiu et al., 2022b). The bias correction with the quantile mapping method is based on the Python module bias_correction 0.4, whose description, installation, and usage are explained at

Table 2. Regional averages of the agroclimatic indicators calculated based on the bias-corrected model data from three WRF simulations. The ensemble mean (first number) as well as the minimum and maximum ensemble member (in parentheses) is listed. Regional averages of the indicators over the climate subregions in CA are also summarized. They are northern CA (NCA), middle CA (MCA), southern CA (SCA), and the mountainous areas (MT). Their scopes are presented in Fig. 1c of Qiu et al. (2022).

	Region				
	CA	NCA	MCA	SCA	MT
GSL (d)					
1986–2005	201.8	173.4	198.6	265.6	98.2
	(201.1/202.4)	(172.2/174.3)	(198.1/199.2)	(265.0/266.8)	(97.4/99.9)
2031–50	215.1	188.7	209.9	278.2	119.4
	(212.7/216.6)	(186.0/190.2)	(207.6/211.6)	(275.3/280.1)	(117.2/121.5)
BEDD (°C)					
1986–2005	2840.1	2498.0	3177.8	3131.9	920.3
	(2833.9/2844.0)	(2491.6/2502.2)	(3169.4/3183.6)	(3128.1/3134.5)	(916.1/925.2)
2031–50	2865.6	2877.8	3233.6	2721.5	1145.7
	(2850.0/2882.5)	(2804.5/2963.1)	(3217.5/3242.8)	(2647.1/2787.0)	(1102.6/11214.9)
FD (d)					
1986–2005	13.9	20.1	7.0	0.6	78.3
	(13.5/14.5)	(19.5/21.2)	(6.4/7.6)	(0.6/0.7)	(77.7/78.7)
2031–50	9.8	12.7	4.2	0.3	63.6
	(9.1/10.1)	(11.8/13.3)	(3.7/4.6)	(0.3/0.4)	(61.1/65.5)
SU (d)					
1986–2005	88.2	48.2	94.8	139.5	5.7
	(88.0/88.4)	(48.1/48.2)	(94.6/94.9)	(139.0/140.1)	(5.6/5.7)
2031–2050	103.6	70.4	111.6	149.6	9.2
	(101.1/107.9)	(65.3/78.7)	(109.9/114.8)	(147.4/153.1)	(8.4/10.7)
WSDI (d)					
1986–2005	21.9	19.8	21.8	22.9	26.0
	(21.6/22.5)	(17.4/21.9)	(21.4/22.0)	(22.1/23.7)	(25.9/26.3)
2031–50	44.7	44.1	44.0	46.0	46.3
	(41.2/51.2)	(36.9/55.0)	(41.0/48.8)	(41.8/51.5)	(42.3/52.4)
TR (d)					
1986–2005	34.8	4.2	31.8	79.4	0.1
	(34.8/34.8)	(4.2/4.2)	(31.8/31.8)	(79.4/79.5)	(0.1/0.1)
2031–50	50.2	13.9	50.9	98.5	0.5
	(48.0/54.2)	(10.7/18.6)	(48.5/55.5)	(96.3/101.9)	(0.3/0.9)

https://pypi.org/project/bias-correction/. The Climate Data Operators (CDO, https://code.mpimet.mpg.de/projects/cdo), Python modules (like netCDF4, Xarray, and Numpy), and NCAR Command Languages (NCL, https://www.ncl.ucar.edu/) are recommended to do operations on the netCDF files.

5. Discussion and conclusion

A high-resolution projection dataset of agroclimatic indicators (AIs) over Central Asia (CA) is derived based on daily mean/maximum/minimum temperature (TG/TX/TN) from the 9-km-resolution dynamically downscaled results of three different GCMs. The AIs used are growing season length (GSL, d), biologically effective degree days (BEDD, °C), frost days (FD, day), summer days (SU, d), warming spell duration index (WSDI, day), and tropical nights (TR, day). The reference and future periods are 1986–2005 and 2031–50, respectively.

The quantile mapping (QM) method is applied to correct the TG/TX/TN from the downscaled results, and then the AIs relating to absolute temperature thresholds are calculated. Comparison between AIs calculated based on the raw and bias-corrected model data (Raw-AIs and Cor-AIs) and those calculated based on the observations (Obs-AIs) shows that the QM method largely reduced the biases in the Raw-AIs. Projected changes in the Cor-AIs during the future period (2031–50) relative to the reference period (1986–2005) are assessed. Results show that GSL, SU, WSDI, and TR will significantly increase over CA and FD will decrease. However, changes in BEDD are spatially heterogeneous.

Model data from Phase 6 of the Coupled Model Intercomparison Project (CMIP6) has been successively released since 2019. Some studies have found that the CMIP6 models bring improvements in simulating the climate in some regions relative to those of CMIP5 (Jiang et al., 2020a; Xin et al., 2020; Dong and Dong, 2021). The dynamical downscaling in this study began in early 2019, and at that point the available model data from CMIP6 that could be used to drive the WRF model was rare. Thus, we chose the CMIP5 models to do the downscaling. The CMIP6 models will be prioritized for the studies in the next stage.

This study assessed projected changes in some key agroclimatic indicators over CA, its climate subregions, and main producing areas of wheat and cotton, to present some
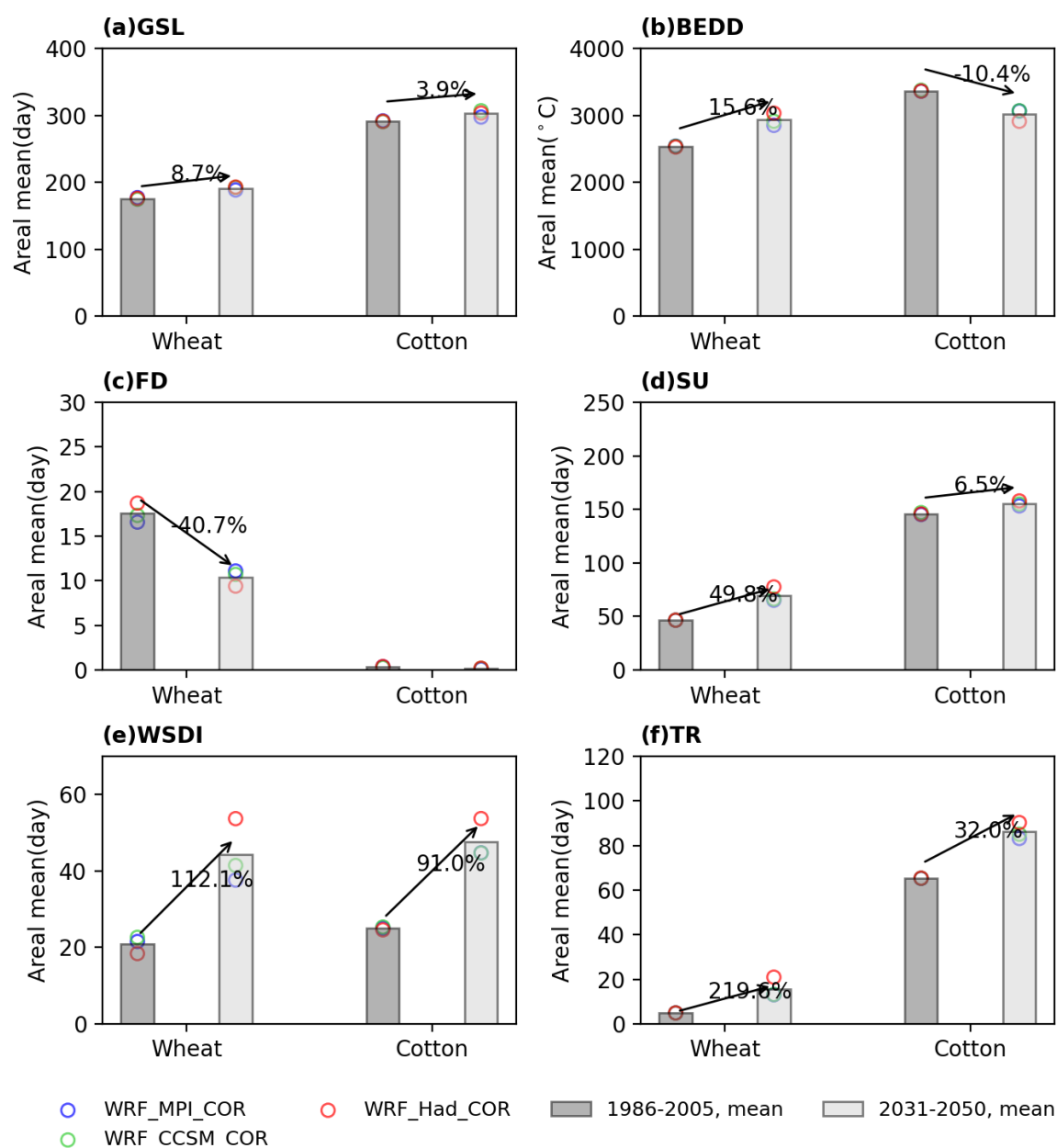
Fig. 6. Areal means of the agroclimatic indicators over the main producing areas of wheat and cotton during the reference (1986–2005) and future (2031–50) periods. The circles are the results of each simulation (WRF_MPI_COR, WRF_CCSM_COR, and WRF_Had_COR), and the bars are the mean values. The digit s are the change ratio.

preliminary results on the potential impact of climate change on the local agriculture. Further studies with dynamic agroecosystem models, such as crop yield models, are recommended to make a more accurate assessment with consideration of limiting crop production factors (e.g., CO_2 fertilization, soil nutrients, and fertility) and viable adaptation options (e.g., irrigation).

suo Project-special fund project in the field of climate, meteorology, and ocean. The produced dataset is provided by the National Tibetan Plateau Data Center (http://data.tpdc.ac.cn).

REFERENCES

Arnell, N. W., and A. Freeman, 2021: The effect of climate change on agro-climatic indicators in the UK. *Climatic Change*, **165**, 40, https://doi.org/10.1007/s10584-021-03054-8.

Aryal, J. P., T. B. Sapkota, R. Khurana, A. Khatri-Chhetri, D. B. Rahut, and M. L. Jat, 2020: Climate change and agriculture in South Asia: Adaptation options in smallholder production systems. *Environment, Development and Sustainability*, **22**, 5045–5075, https://doi.org/10.1007/s10668-019-00414-4.

Ashfaq, M., L. C. Bowling, K. Cherkauer, J. S. Pal, and N. S. Diffenbaugh, 2010: Influence of climate model biases and daily-scale temperature and precipitation events on hydrological impacts assessment: A case study of the United States. *J. Geophys. Res.*, **115**, D14116, https://doi.org/10.1029/2009JD012965.

Babu, S. C., and S. Djalalov, 2006: *Policy Reforms and Agriculture Development in Central Asia*. Springer, https://doi.org/10.1007/0-387-29779-0.

Bandara, J. S., and Y. Y. Cai, 2014: The impact of climate change on food crop productivity, food prices and food security in South Asia. *Economic Analysis and Policy*, **44**, 451–465, https://doi.org/10.1016/j.eap.2014.09.005.

Bruyère, C. L., J. M. Done, G. J. Holland, and S. Fredrick, 2014: Bias corrections of global models for regional climate simulations of high-impact weather. *Climate Dyn.*, **43**, 1847–1856, https://doi.org/10.1007/s00382-013-2011-6.

Chen, F. H., J. S. Wang, L. Y. Jin, Q. Zhang, J. Li, and J. H. Chen, 2009: Rapid warming in mid-latitude central Asia for the past 100 years. *Frontiers of Earth Science in China*, **3**, 42, https://doi.org/10.1007/s11707-009-0013-9.

Chen, F. H., W. Huang, L. Y. Jin, J. H. Chen, and J. S. Wang, 2011: Spatiotemporal precipitation variations in the arid Central Asia in the context of global warming. *Science China Earth Sciences*, **54**, 1812–1821, https://doi.org/10.1007/s11430-011-4333-8.

Cramer, W., and Coauthors, 2018: Climate change and interconnected risks to sustainable development in the Mediterranean. *Nature Climate Change*, **8**, 972–980, https://doi.org/10.1038/s41558-018-0299-2.

Dong, T. Y., and W. J. Dong, 2021: Evaluation of extreme precipitation over Asia in CMIP6 models. *Climate Dyn.*, **57**, 1751–1769, https://doi.org/10.1007/s00382-021-05773-1.

Dosio, A., 2016: Projections of climate change indices of temperature and precipitation from an ensemble of bias-adjusted high-resolution EURO-CORDEX regional climate models. *J. Geophys. Res.*, **121**, 5488–5511, https://doi.org/10.1002/2015JD024411.

Gessner, U., V. Naeimi, I. Klein, C. Kuenzer, D. Klein, and S. Dech, 2013: The relationship between precipitation anomalies and satellite-derived vegetation activity in Central Asia. *Global and Planetary Change*, **110**, 74–87, https://doi.org/10.1016/j.gloplacha.2012.09.007.

Giorgi, F., 2006: Climate change hot-spots. *Geophys. Res. Lett.*, **33**, L08707, https://doi.org/10.1029/2006GL025734.

Gudmundsson, L., J. B. Bremnes, J. E. Haugen, and T. Engen-Skau-

gen, 2012: Technical Note: Downscaling RCM precipitation to the station scale using statistical transformations – a comparison of methods. *Hydrology and Earth System Sciences*, **16**, 3383–3390, https://doi.org/10.5194/hess-16-3383-2012.

Hersbach, H., and Coauthors, 2020: The ERA5 global reanalysis. *Quart. J. Roy. Meteor. Soc.*, **146**, 1999–2049, https://doi.org/10.1002/qj.3803.

Holden, N. M., and A. J. Brereton, 2004: Definition of agroclimatic regions in Ireland using hydro-thermal and crop yield data. *Agricultural and Forest Meteorology*, **122**, 175–191, https://doi.org/10.1016/j.agrformet.2003.09.010.

Hu, Z. Y., C. Zhang, Q. Hu, and H. Q. Tian, 2014: Temperature changes in central Asia from 1979 to 2011 based on multiple datasets. *J. Climate*, **27**, 1143–1167, https://doi.org/10.1175/jcli-d-13-00064.1.

Hu, Z. Y., Q. M. Zhou, X. Chen, C. Qian, S. S. Wang, and J. F. Li, 2017: Variations and changes of annual precipitation in Central Asia over the last century. *International Journal of Climatology*, **37**, 157–170, https://doi.org/10.1002/joc.4988.

Huang, A. N., Y. Zhou, Y. C. Zhang, D. Q. Huang, Y. Zhao, and H. M. Wu, 2014: Changes of the annual precipitation over central asia in the twenty-first century projected by multimodels of CMIP5. *J. Climate*, **27**, 6627–6646, https://doi.org/10.1175/jcli-d-14-00070.1.

Huang, M. X., J. Wang, B. Wang, D. L. Liu, Q. Yu, D. He, N. Wang, and X. B. Pan, 2020: Optimizing sowing window and cultivar choice can boost China's maize yield under 1.5°C and 2°C global warming. *Environmental Research Letters*, **15**, 024015, https://doi.org/10.1088/1748-9326/ab66ca.

Iglesias, A., R. Mougou, M. Moneo, and S. Quiroga, 2011: Towards adaptation of agriculture to climate change in the Mediterranean. *Regional Environmental Change*, **11**, 159–166, https://doi.org/10.1007/s10113-010-0187-4.

International Food Policy Research Institute, 2019: Global spatially-disaggregated crop production statistics data for 2010 version 2.0. Harvard Dataverse, V4. https://doi.org/10.7910/DVN/PRFF8V.

Iturbide, M., A. Casanueva, J. Bedia, S. Herrera, J. Milovac, and J. M. Gutiérrez, 2022: On the need of bias adjustment for more plausible climate change projections of extreme heat. *Atmospheric Science Letters*, **23**, e1072, https://doi.org/10.1002/asl.1072.

Jiang, D. B., D. Hu, Z. P. Tian, and X. M. Lang, 2020a: Differences between CMIP6 and CMIP5 models in simulating climate over China and the East Asian Monsoon. *Adv. Atmos. Sci.*, **37**, 1102–1118, https://doi.org/10.1007/s00376-020-2034-y.

Jiang, J., T. J. Zhou, X. L. Chen, and L. X. Zhang, 2020b: Future changes in precipitation over Central Asia based on CMIP6 projections. *Environmental Research Letters*, **15**, 054009, https://doi.org/10.1088/1748-9326/ab7d03.

Jiang, Q., and Coauthors, 2021: Evaluation of the ERA5 reanalysis precipitation dataset over Chinese Mainland. *Journal of Hydrology*, **595**, 125660, https://doi.org/10.1016/j.jhydrol.2020.125660.

Lu, X. Y., G. Q. Tang, X. C. Liu, X. Q. Wang, Y. Liu, and M. Wei, 2021: The potential and uncertainty of triple collocation in assessing satellite precipitation products in Central Asia. *Atmospheric Research*, **252**, 105452, https://doi.org/10.1016/j.atmosres.2021.105452.

Mannig, B., and Coauthors, 2013: Dynamical downscaling of climate change in Central Asia. *Global and Planetary Change*, **110**, 26–39, https://doi.org/10.1016/j.gloplacha.2013.05.

008.

Mirzabaev, A., 2018: Improving the resilience of central asian agriculture to weather variability and climate change. *Climate Smart Agriculture*: *Building Resilience to Climate Change*, L. Lipper, et al., Eds., Springer, 477–495, https://doi.org/10.1007/978-3-319-61194-5_20.

Mountain Research Initiative EDW Working Group., 2015: Elevation-dependent warming in mountain regions of the world. *Nature Climate Change*, **5**, 424–430, https://doi.org/10.1038/nclimate2563.

Ozturk, T., M. T. Turp, M. Türkeş, and M. L. Kurnaz, 2017: Projected changes in temperature and precipitation climatology of Central Asia CORDEX Region 8 by using RegCM4.3.5. *Atmos. Res.*, **183**, 296–307, https://doi.org/10.1016/j.atmosres.2016.09.008.

Palazzi, E., L. Mortarini, S. Terzago, and J. von Hardenberg, 2019: Elevation-dependent warming in global climate model simulations at high spatial resolution. *Climate Dyn.*, **52**, 2685–2702, https://doi.org/10.1007/s00382-018-4287-z.

Peng, D. D., T. J. Zhou, L. X. Zhang, and L. W. Zou, 2019: Detecting human influence on the temperature changes in Central Asia. *Climate Dyn.*, **53**, 4553–4568, https://doi.org/10.1007/s00382-019-04804-2.

Petr, J., 1991: *Weather and Yield* (*Developments in Crop Science 20*). Elsevier, 288 pp.

Piani, C., J. O. Haerter, and E. Coppola, 2010: Statistical bias correction for daily precipitation in regional climate models over Europe. *Theoretical and Applied Climatology*, **99**, 187–192, https://doi.org/10.1007/s00704-009-0134-9.

Piao, S. L., and Coauthors, 2010: The impacts of climate change on water resources and agriculture in China. *Nature*, **467**, 43–51, https://doi.org/10.1038/nature09364.

Qiu, Y., 2022: High-resolution projection dataset of agroclimatic indicators over Central Asia (1986–2005 and 2031–2050). National Tibetan Plateau Data Center, http://doi.org/10.11888/Atmos.tpdc.271934.

Qiu, Y., J. M. Feng, Z. W. Yan, J. Wang, and Z. Li, 2022a: High-resolution dynamical downscaling for regional climate projection in Central Asia based on bias-corrected multiple GCMs. *Climate Dyn.*, **58**, 777–791, https://doi.org/10.1007/s00382-021-05934-2.

Qiu, Y., Feng, J., Yan, Z., and Wang, J, 2022b: HCPD-CA: high-resolution climate projection dataset in central Asia. *Earth Syst. Sci. Data*, **14**, 2195–2208, https://doi.org/10.5194/essd-14-2195-2022.

Rangwala, I., E. Sinsky, and J. R. Miller, 2013: Amplified warming projections for high altitude regions of the northern hemisphere mid-latitudes from CMIP5 models. *Environmental Research Letters*, **8**, 024040, https://doi.org/10.1088/1748-9326/8/2/024040.

Rijks, D., 1994: Agroclimatic characterization. *Handbook of Agricultural Meteorology*. J. E. Griffiths, Ed., Oxford University Press, 231–244.

SIS, C. S. G. A., 2019: Agroclimatic Indicators Algroithm Theretical Basis Document (ATBD).

Skamarock, W. C., and Coauthors, 2008: A description of the Advanced Research WRF version 3. No. NCAR/TN-475+STR, https://doi.org/10.5065/D68S4MVH.

Sommer, R., and Coauthors, 2013: Impact of climate change on wheat productivity in Central Asia. *Agriculture, Ecosystems & Environment*, **178**, 78–99, https://doi.org/10.1016/j.agee.2013.06.011.

Teutschbein, C., and J. Seibert, 2012: Bias correction of regional climate model simulations for hydrological climate-change impact studies: Review and evaluation of different methods. *J. Hydrol.*, **456–457**, 12–29, https://doi.org/10.1016/j.jhydrol.2012.05.052.

Themeßl, M. J., A. Gobiet, and A. Leuprecht, 2011: Empirical-statistical downscaling and error correction of daily precipitation from regional climate models. *International Journal of Climatology*, **31**, 1530–1544, https://doi.org/10.1002/joc.2168.

Thurman, M., 2011: Natural disaster risks in Central Asia: A synthesis.

Tong, Y., X. J. Gao, Z. Y. Han, Y. Q. Xu, Y. Xu, and F. Giorgi, 2021: Bias correction of temperature and precipitation over China for RCM simulations using the QM and QDM methods. *Climate Dyn.*, **57**, 1425–1443, https://doi.org/10.1007/s00382-020-05447-4.

Trnka, M., and Coauthors, 2011: Expected changes in agroclimatic conditions in Central Europe. *Climatic Change*, **108**, 261–289, https://doi.org/10.1007/s10584-011-0025-9.

Wang, J. X., R. Mendelsohn, A. Dinar, J. K. Huang, S. Rozelle, and L. J. Zhang, 2009: The impact of climate change on China's agriculture. *Agricultural Economics*, **40**, 323–337, https://doi.org/10.1111/j.1574-0862.2009.00379.x.

Wang, Y. L., J. M. Feng, M. Luo, J. Wang, and Y. Qiu, 2020: Uncertainties in simulating central Asia: Sensitivity to physical parameterizations using Weather Research and Forecasting model. *International Journal of Climatology*, **40**, 5813–5828, https://doi.org/10.1002/joc.6567.

Xin, X. G., T. W. Wu, J. Zhang, J. C. Yao, and Y. J. Fang, 2020: Comparison of CMIP6 and CMIP5 simulations of precipitation in China and the East Asian summer monsoon. *International Journal of Climatology*, **40**, 6423–6440, https://doi.org/10.1002/joc.6590.

Xue, C. D., H. Wu, and X. G. Jiang, 2019: Temporal and spatial change monitoring of drought grade based on ERA5 analysis data and BFAST method in the belt and road area during 1989–2017. *Advances in Meteorology*, **2019**, 4053718, https://doi.org/10.1155/2019/4053718.

Zhu, X., Z. G. Wei, W. J. Dong, Z. M. Ji, X. H. Wen, Z. Y. Zheng, D. D. Yan, and D. L. Chen, 2020: Dynamical downscaling simulation and projection for mean and extreme temperature and precipitation over central Asia. *Climate Dyn.*, **54**, 3279–3306, https://doi.org/10.1007/s00382-020-05170-0.